Acta Pharmaceutica Sinica B 2024;14(9):4059–4072

Chinese Pharmaceutical Association
Institute of Materia Medica, Chinese Academy of Medical Sciences

Acta Pharmaceutica Sinica B

www.elsevier.com/locate/apsb
www.sciencedirect.com

ORIGINAL ARTICLE

CRISPR-Cas9 gene editing strengthens cuproptosis/chemodynamic/ferroptosis synergistic cancer therapy

Xiaoyu Wu[a,†], Zijun Bai[b,†], Hui Wang[d,†], Hanqing Wang[e], Dahai Hou[b], Yunzhu Xu[b], Guanqun Wo[b], Haibo Cheng[c,*], Dongdong Sun[c,*], Weiwei Tao[b,*]

[a]*Department of Surgical Oncology, Affiliated Hospital of Nanjing University of Chinese Medicine, Nanjing 210029, China*
[b]*School of Integrated Medicine, Nanjing University of Chinese Medicine, Nanjing 210023, China*
[c]*Jiangsu Collaborative Innovation Center of Traditional Chinese Medicine in Prevention and Treatment of Tumor, Nanjing University of Chinese Medicine, Nanjing 210023, China*
[d]*School of Pharmacology, Nanjing University of Chinese Medicine, Nanjing 210023, China*
[e]*School of Pharmacology, Ningxia Medical University, Yinchuan 750004, China*

Received 21 February 2024; received in revised form 15 May 2024; accepted 16 May 2024

KEY WORDS

GSH- and pH-responsive;
Effective copper delivery;
CRISPR-Cas9;
ATP7A;
Cuproptosis;
Chemodynamic;
Ferroptosis;
Synergistic therapy

Abstract Copper-based nanomaterials demonstrate promising potential in cancer therapy. Cu^{+} efficiently triggers a Fenton-like reaction and further consumes the high level of glutathione, initiating chemical dynamic therapy (CDT) and ferroptosis. Cuproptosis, a newly identified cell death modality that represents a great prospect in cancer therapy, is activated. However, active homeostatic systems rigorously keep copper levels within cells exceptionally low, which hinders the application of cooper nanomaterials-based therapy. Herein, a novel strategy of CRISPR-Cas9 RNP nanocarrier to deliver cuprous ions and suppress the expression of copper transporter protein ATP7A for maintaining a high level of copper in cytoplasmic fluid is developed. The Cu_2O and organosilica shell would degrade under the high level of glutathione and weak acidic environment, further releasing RNP and Cu^{+}. The liberated Cu^{+} triggered a Fenton-like reaction for CDT and partially transformed to Cu^{2+}, consuming intracellular GSH and initiating cuproptosis and ferroptosis efficiently. Meanwhile, the release of RNP effectively reduced the expression of copper transporter ATP7A, subsequently increasing the accumulation of cooper

*Corresponding authors.
E-mail addresses: hbcheng_njucm@163.com (Haibo Cheng), sundd@njucm.edu.cn (Dongdong Sun), taoww@njucm.edu.cn (Weiwei Tao).
[†]These authors made equal contributions to this work.
Peer review under the responsibility of Chinese Pharmaceutical Association and Institute of Materia Medica, Chinese Academy of Medical Sciences.

https://doi.org/10.1016/j.apsb.2024.05.029

and enhancing the efficacy of CDT, cuproptosis, and ferroptosis. Such tumor microenvironment responsive multimodal nanoplatform opens an ingenious avenue for colorectal cancer therapy based on gene editing enhanced synergistic cuproptosis/CDT/ferroptosis.

1. Introduction

Colorectal cancer (CRC) is one of the advanced cancers with high incidence and mortality rates worldwide due to its low early diagnosis rate, high risk of recurrence and metastasis, and inadequate therapy[1,2]. Currently, the treatment of CRC is mainly relying on surgery, supplemented by postoperative radiotherapy, chemotherapy, and immunotherapy. However, after traditional treatment modalities, patients have poor postoperative recovery and serious side effects[3]. Therefore, it is urgent to develop new efficient medicines for conquering the shortcomings of the present CRC treatment.

Copper is an indispensable trace element that maintains the normal operation of the body and participates in the physiological processes of almost all types of cells[4]. Maintaining a dynamic balance of copper ions is crucial, as imbalance leads to oxidative stress, abnormal autophagy, and various copper ion-related diseases. Patients with cancers, like breast, lung, prostate, and colorectal cancers, often exhibit elevated copper levels in tumors or serum. Excessive copper accumulation can be life-threatening, but controlled increases in cellular copper levels show potential for selectively killing cancer cells. Recently, a new mechanism called "cuproptosis" has been discovered, which is obviously different from the known controlled death modes such as apoptosis, pyroptosis, necroptosis, and ferroptosis[5]. Specifically, copper death is the breakdown of intracellular copper homeostasis and the combination of accumulated cuprous ions with lipoylated components of the tricarboxylic acid cycle, resulting in aggregation of lipoylated proteins and loss of Fe−S cluster proteins[6,7]. Besides, cuprous ions could also trigger the Fenton-like reaction to transform the hydrogen peroxide (H_2O_2) into highly cytotoxic reactive oxygen species (ROS), which makes the occurrence of chemical dynamic therapy (CDT)[8,9]. Notably, Cu-catalyzed Fenton-like reactions are highly effective in mildly acidic and neutral environments, exhibiting a catalytic efficiency approximately 160 times higher than that of Fe[10]. Additionally, Cu^+/Cu^{2+} possesses a lower redox potential compared to Fe^{2+}/Fe^{3+}, facilitating the Cu^+/Cu^{2+} cycle-mediated completion of the H_2O_2[11]. Furthermore, Cu^+/Cu^{2+} readily converts excess reduced glutathione (GSH) to glutathione disulfide (GSSG) during the valence conversion process[12,13]. The activity of the GPX4 enzyme is inhibited, which subsequently induces the accumulation of lipid peroxidation (LPO) and promotes ferroptosis in tumor cells[14–16]. In summary, copper-based nanomedicine could simultaneously activate cuproptosis, CDT, and ferroptosis, and may achieve great therapeutic efficacy by a synergistic effect.

However, active homeostatic systems rigorously keep copper levels within cells exceptionally low[17]. The copper-transporting ATP7A (the main exporter that controls copper efflux) is responsible for removing the extra copper from cells to avoid free copper accumulation[18]. As a result, it is difficult to maintain a high level of copper in cytoplasmic fluid for effective cuproptosis/CDT/ferroptosis. Thus, a strategy for suppressing the expression of copper transporter protein ATP7A is in great demand. Recently, CRISPR-Cas9 has been considered as a powerful tool for achieving controllable gene editing due to its flexible release within the cell nucleus, minimal off-target effects, and low cellular toxicity[19]. Generally, both physical and viral vectors have been explored to deliver CRISPR-Cas9 components for *in vitro* experiments, but they do not meet the requirements for *in vivo* applications. Viral vectors also face limitations of inherent defects such as insertional mutations, immunogenicity, and ineffective packaging capacity[20,21]. To overcome the abovementioned issues, tremendous nanomaterials with tumor microenvironment (TME) responsive ability have been established for efficient CRISPR-Cas9 components delivery through the enhanced permeability and retention (EPR) effect[22]. Previous studies have exhibited that nanomaterials such as CuS, Au nanooctopus, and Au nanorods loaded with CRISPR-Cas9 components can realize the controlled release for efficient gene editing, finally inhibiting the expression of heat shock proteins (HSPs) and achieving synergistic mild photothermal therapy (PTT) effects[23–25]. Thus, for the sake of elevating the cancer therapy effect of Cu-based nanomaterials, an ingenious design of CRISPR-Cas9 nanocarrier that delivers cuprous ions and suppresses the expression of copper transporter protein ATP7A for maintaining a high level of copper in cytoplasmic fluid have been a significant portion to implement the gene editing enhanced cuproptosis/CDT/ferroptosis synergistic therapy.

In this study, we established a multimodal therapeutic nanoplatform, RNP@Cu_2O@SPF, which can efficiently transport CRISPR-Cas9-Sg*ATP7A* (RNP) and cuprous ions in response to TME. Initially, Cu_2O nanoparticle was synthesized to provide the cuprous ions and utilized as carriers for RNP delivery. Then, the GSH degradable organosilica shell was coated to prevent RNP leakage, and folic acid (FA) was finally modified *via* the condensation of hydroxyl and amino groups. The constructed nanomedicine entered the cytoplasm after endosomal escapes due to the EPR and FA-mediated active targeting effect. Intracellular high-level GSH and weak acid environment triggered the degradation of the organosilica network and Cu_2O, releasing RNP and Cu^+. RNP specifically reduced the expression of copper transporter ATP7A, resulting in the accumulation of copper in the cytoplasm. Simultaneously, the accumulated cooper triggered the Fenton-like reaction cycle, expanding GSH and initiating copper-dependent therapies, including CDT, ferroptosis, and cuproptosis. Thus, this RNP@Cu_2O@SPF therapeutic nanoplatform has promising potential for CRC therapy based on gene editing enhanced synergistic cuproptosis/CDT/ferroptosis.

2. Materials and methods

2.1. Chemicals and materials

All chemicals were accessible on the market, and all of them were utilized without further purification. Sodium hydroxide (NaOH,

97%), copper acetate monohydrate ($Cu(Ac)_2 \cdot H_2O$), ascorbic acid (AA), methylene blue (MB), bis 3-(triethoxysilyl)propyl tetrasulfide (BTES), tetraethyl orthosilicate (TEOS, 98%), 1-ethyl-3-(3-dimethylaminopropyl) carbodiimide hydrochloride (EDC, ≥98%), *n*-hydroxysuccinimide (NHS, 98%), 3-aminopropyl triethoxysilane (APTES), fluorescein isothiocyanate (FITC, 95%), rhodamine B Isothiocyanate (RITC, 95%), glutathione (GSH, 98%), 5,5′-dithiobis (2-nitrobenzoic acid) (DTNB), 2′,7′-dichlorodihydrofluorescein diacetate (DCFH-DA, ≥97%), 3-(4,5-dimethylthiazol-2-yl)-2,5-diphenyltetrazolium bromide (MTT, 98%), hoechst (98%), 4′,6-diamidino-2-phenylindole (DAPI) and the annexin V-FITC/PI apoptosis detection kit were acquired from Sigma−Aldrich (USA). Ammonium hydroxide, Triton X-100, cyclohexane, polyethylene glycol (PEG, 6000 Da), FA-PEG-COOH (3400 Da, 95%), hydrogen peroxide (H_2O_2, 30%) and *n*-hexane were purchased from Aladdin Industries Inc. (Shanghai, China). The GSH/GSSG assay kit was purchased from Beyotime Co., Ltd. (Shanghai, China).

Anti-ATP7A antibody (PA5-103110) was purchased from ThermoFisher (MA, USA). Anti-FDX1 antibody (abs137427) was purchased from absin (Shanghai, China). Anti-LIAS (ab96302), anti-ACO-2 (ab129105), and anti-SDHB9 (ab14714) antibodies were purchased from Abcam (MA, USA). Anti-DLAT (12362), anti-Tubulin (2128), anti-rabbit IgG (H+L) (14708), and anti-mouse IgG (H+L) (14709) antibodies were purchased from CST (MA, USA).

2.2. Characterizations

The morphology and elemental mapping of the synthesized nanoparticles were characterized by scanning electron microscopy (SEM, Hitachi S4800, JEOL Ltd., Japan) with voltages of 5−15 kV. The UV−Vis absorption spectrum was collected by Lambda 750 spectrophotometer (PerkinElmer Enterprise Management Co., Ltd., Shanghai, China). A Malvern Zetasizer (Zetasizer Nano ZS, Malvern, UK) was used to characterize the size and zeta potential of the prepared nanoparticles. Confocal fluorescence images of cells were captured by a confocal laser scanning microscope (Olympus IX 70, Japan). Animal images were taken by an E50 IR camera (FLIR, Arlington, VA). The flow cytometry experiments were conducted on the flow cytometer (Guava easyCyteTM).

2.3. Synthesis of Cu_2O nanoparticles

Cu_2O nanoparticles were prepared according to the previous work[26]. Specifically, PEG (2 g) was first dissolved in 50 mL of $Cu(Ac)_2 \cdot H_2O$ aqueous solution (0.01 mol/L). Afterward, 0.2 mL of NaOH solution (6.0 mol/L) was slowly injected into the above solution and stirred for 30 min. Then, 1 mL of AA aqueous solution (1 mol/L) was added drop by drop and reacted for 1 h. The synthesized Cu_2O nanoparticles were centrifuged and washed three times with ultrapure water and dried under vacuum (60 °C, 12 h).

2.4. FITC-labeled Cas9

Cas9 was combined with NHS and EDC in a buffer containing 4-(2-hydroxyethyl)-1-piperazine ethanesulfonic acid (HEPES, pH 5.5) and incubated for 30 min. Subsequently, FITC was introduced to the solution, agitated continuously for 3 h, and FITC-labeled Cas9 was harvested by dialysis.

2.5. Synthesis of Cas9/sgRNA (RNP)

The synthesis method of Cas9 protein and sgRNA (*ATP7A*) was according to the reported preparation process. Cas9 and sgRNA (weight ratio 3:1) were added into Tris−HCl buffer and incubated at room temperature for 15 min to prepare Cas9/sgRNA complex (RNP). The sgRNA sequence of the *ATP7A* target site was: 5′-GGTGAAGAGTTGCAAAGTGG-3′.

2.6. Synthesis of RNP@Cu_2O@SPF nanoparticles

The aforementioned prepared Cu_2O nanoparticles were redispersed in HEPES buffer (pH 7.4), and different concentrations (200, 400, and 800 μg/mL) of FITC-labeled RNP were added. After 12 h of stirring in the dark, the RNP was loaded on the surface of Cu_2O nanoparticles due to the electrostatic interaction. The organosilica shell synthesis process was referred to a previous report[27]. Firstly, Triton X-100 (1.0 mL) and *n*-hexanol (1.0 mL) were dissolved in cyclohexane (4.0 mL), then 50 μL of RNP@Cu_2O aqueous solution was mixed with 20 μL of TEOS and 30 μL of BTES. After shaking, this mixture was added to the previous organic medium. Eventually, 20 μL of 25% ammonia aqueous solution was added and stirred for 12 h at room temperature. Finally, the obtained nanoparticles (RNP@Cu_2O@S) were centrifuged and washed several times with water and ethanol. For FA-PEG-COOH modification, the RNP@Cu_2O@S nanoparticles were dispersed in the ethanol, and 10 μL APTES was added and stirred for 4 h to modify the amino group on the surface of organosilica. Then the nanoparticles were washed with ethanol and water sequentially and redispersed in Tris−HCl buffer, EDC, NHS. FA-PEG-COOH were injected for the condensation reaction of amino and carboxyl groups. Finally, the fabricated RNP@Cu_2O@SPF nanoparticles were washed three times with water.

2.7. RITC-labeled RNP@Cu_2O@SPF nanoparticles

At room temperature, RNP@Cu_2O@SPF nanoparticles and RITC were added to the HEPES buffer and stirred in the dark for 8 h. Then, the mixture was centrifuged. RITC-labeled RNP@Cu_2O@SPF particles were obtained after three times of washes.

2.8. Release of RNP

The release ability of FITC labeled RNP from RNP@Cu_2O@SPF nanoparticles was measured by recording the fluorescence intensities of the supernatant at different GSH and pH conditions.

2.9. Release of ion

1 mL of RNP@Cu_2O@SPF (1 mg/mL) was dispersed in a dialysis bag (MWCO: 2000 Da) contrasting with 49 mL PBS buffer (with GSH and various pH conditions). After incubation for different times, 1 mL of dialysate was taken out for quantification. The total content of Cu in RNP@Cu_2O@SPF was calculated with the help of excess GSH and HCl for completely dissolution. Quantification was performed by ICP-MS (PerkinElmer, ELAN DRC-II, USA).

2.10. GSH depletion assay

DTNB was used as a probe to detect the consumption of GSH by RNP@Cu_2O@SPF. Different amounts of RNP@Cu_2O@SPF and GSH (10 mmol/L) were incubated for 4 h at 37 °C. After the

mixture was centrifuged for 10 min, the supernatant was collected and DNTB was added for reacting with 10 min. The absorbance at 412 nm was measured using an UV−Vis (PerkinElmer) spectrophotometer.

2.11. ROS generation detection

MB was used to detect the generation of hydroxyl radical (·OH). The PBS (pH 5.0) buffer with GSH (10 mmol/L) was reacted with the following substances at 37 °C for 30 min: (1) MB; (2) MB + H_2O_2; (3) MB + H_2O_2 + RNP@Cu_2O@SPF (H_2O_2 10 mmol/L). The supernatant was then extracted, and an UV−Vis spectrophotometer was used to measure the ultraviolet absorption.

2.12. Cell uptake of nanoparticles

CRC cell line SW480 was added to a medium containing 10% fetal bovine serum (FBS, Lonsera, S711−001S), 1% penicillin, and 1% streptomycin (Beyotime, KGY002), cultured for 12 h in a humidified incubator with 5% carbon dioxide, and then treated with different nanoparticle. To monitor the cell uptake process, FITC and RITC were used to label RNP and RNP@Cu_2O@SPF, respectively. After incubation for 4 h, the culture medium was replaced. The nucleus was then stained for 15 min with Hoechst 33342. After CLSM fluorescence observation, the uptake of the nanoparticle was measured by flow cytometry.

2.13. Cell cytotoxicity assay

SW480 cells were seeded at a density of 5×10^3 cells/well in a 96-well plate and cultured for 24 h to allow for attachment. Then, the initial medium was replaced with a fresh medium containing nanoparticles at various concentrations. After 24 h, the supernatant was discarded, and the cells were washed twice with PBS. 100 μL of fresh medium containing MTT (0.5 mg/mL) was added, followed by an additional 4 h incubation. Absorbance was then measured at 570 nm using a microplate reader (Multiskan Sky, Thermo Fisher, USA).

2.14. Intracellular ROS generation

The cells were first inoculated in a 24-well plate at a density of 2.5×10^5 cells per well and incubated for 24 h to make them adhere to the wall. After removing the medium, the cells were exposed to the following substances for 24 h: Cu_2O@SPF (40 μg/mL), RNP@Cu_2O@SPF (40 μg/mL), and RNP@Cu_2O@SPF (80 μg/mL). Subsequently, the cells were incubated with DCFH-DA for 30 min and washed with PBS twice. Finally, Hoechst staining was performed for 5 min, followed by fluorescence observation. Quantitative detection was performed by flow cytometry.

2.15. Cu ion content detection

The Cell Copper (Cu) Colorimetric Assay Kit (Elabscience Biotechnology, Wuhan, China) was selected to detect the copper ion content in SW480 cells, and the BCA Protein Colorimetric Assay Kit (Elabscience Biotechnology, Wuhan, China) was also used to determine the total protein concentration. PBS, Cu_2O@SPF, and RNP@Cu_2O@SPF were added to the standard wells and assay wells, followed by 50 μL of chromogenic reagent working solution. The wells were covered with a film and incubated at 37 °C for 5 min. The enzyme labeling The OD value of each well was measured at 580 nm. According to the calculation formula for copper ion concentration, the intracellular Cu ion content was calculated.

2.16. GSH/GSSG ratio detection

A GSH and GSSG Assay Kit was used to measure the GSH/GSSG ratio in cells after administration of different concentrations of RNP@Cu_2O@SPF. After fully mixing the prepared GSH/GSSG standard samples and experimental reagents, they were incubated at room temperature for 10 min. The absorbance was then detected in the range of 405−415 nm using a microplate reader (Thermo Fisher).

2.17. Cell colony and migration assays

2×10^3 SW480 cells were inoculated into a sterile 6-well plate. After 24 h of adhesion, the cells were treated with different nanopreparations and cultured in a CO_2 incubator at 37 °C for 2 weeks. When visible spots were formed, the culture medium was discarded. Cells were fixed with methanol for 30 min and stained with 2 mL of 0.1% crystal violet for 30 min. After washing off, pictures were taken with a digital camera (Nikon D750, Japan), and counted colonies.

To study cell invasion, Matrigengel was thawed in a 4 °C refrigerator in advance, and the materials used in the experiment were pre-cooled at 4 °C. The Matrigel dilution (40 μL/well) was absorbed and added vertically to the upper chamber of a 24-well Transwell with a pore size of 8 μm. It was then incubated at 37 °C for 30 min to solidify. The treated SW480 cell suspension was used at a density of 2×10^5 cells per well. Cells were inoculated into the upper chamber, and medium containing 10% FBS was added to the lower chamber. After 24 h of incubation, the cells were taken out, the culture medium in the well was discarded, the lower surface was fixed in 70% methanol solution for 30 min, and stained with 0.1% crystal violet for 20 min. Subsequently, the cells were counted under a microscope. Afterward, count under a microscope.

2.18. Cell apoptosis assay

SW480 cells were seeded in 6-well plates at a density of 1×10^5 cells per well and incubated at 37 °C for 24 h. Following incubation, the cells were rinsed with PBS and subjected to staining with Annexin V-YF488 and propidium iodide (PI), according to the manufacturer's instructions. Flow cytometry was then employed to analyze the fluorescence intensity, with the FITC channel utilized for annexin V-FITC detection and the PE channel for PI.

2.19. Intracellular lipid peroxidation (LPO) assay

To assess the level of intracellular LPO after administration of different concentrations of RNP@Cu_2O@SPF, SW480 cells were suspended and washed, and then exposed to a LPO fluorescence assay kit at room temperature, incubated at 37 °C in the dark for 45 min, and washed twice with the working solution. The cells were resuspended and transferred to a microplate reader (Thermo Fisher) for quantitative detection at an excitation wavelength of 500 nm and a detection wavelength of 525 nm.

2.20. Immunofluorescence and Western blot analysis

After washing, fixing, and permeabilizing, SW480 cells were blocked with 1% BSA for 30 min at room temperature, labeled with specific primary antibodies for 12 h at 4 °C, followed by incubation with the corresponding fluorescently labeled secondary antibodies for 1 h. The cells were stained with DAPI for 5 min, washed 2−3 times with PBS, and subjected to CLSM imaging. Cellular proteins in SW480 cells were analyzed using western blotting (WB). Cells were seeded into 24-well plates and treated with various samples for 24 h. After washing with PBS, cells were lysed with RIPA buffer containing protease inhibitors for 30 min on ice. Protein concentration was quantified using the BCA protein assay kit. The proteins were separated on a 12% SDS/PAGE gel and transferred to a PVDF membrane. The membrane was blocked with 5% skimmed milk at room temperature for 1 h, then incubated with primary antibodies for 12 h at 4 °C. The next day, the membrane was incubated with secondary antibody for 1 h, washed with TBST buffer, and finally subjected to exposure.

2.21. Animal tumor models

All operations and postoperative animal care were performed in accordance with the standards of the Animal Care Institutional Committee of Nanjing University of Chinese Medicine (Animal Ethics Committee Accreditation Number: 202302A055). An *in vivo* study was carried out by transplanting tumor SW480 cells into nude mice. 1×10^7 SW480 cells were added to 200 μL PBS and subcutaneously injected into the armpit of male nude mice to establish the SW480 tumor model. The male nude mice were purchased from Changzhou Cavens Experimental Animal Center.

2.22. In vivo biodistribution

To track the *in vivo* biodistribution of targeted or non-targeted nanomedicines, BALB/c tumor-bearing mice with tumor volumes reaching approximately 100 mm^3 were selected for intravenous injection of RNP@Cu_2O@SPF and RNP@Cu_2O@S nanomedicines and *in vivo* imaging ($n = 6$). The system captures NIR fluorescence images at preset time points (1, 4, 12, 24 and 48 h). 48 h after the injection, mice were euthanized, and tumors, hearts, spleens, livers, lungs, and kidneys were harvested for *Ex vivo* imaging (ProteinSimple, CA, USA).

2.23. Tissue accumulation and elimination of RNP@Cu_2O@SPF

ICP-MS was employed to measure the concentrations of Cu and Si, facilitating further assessment of the accumulation of RNP@Cu_2O@SPF *in vivo*. Subcutaneous tumor-bearing mice were immolated at 4, 12, 24, 48, and 72 h separately after tail intravenous injection of RNP@Cu_2O@SPF for biodistribution assessment. Main organs and tumors were then collected, processed, and analyzed using ICP-MS (PerkinElmer).

2.24. Antitumor analysis

BALB/c tumor-bearing mice with a tumor volume of about 100 mm^3 were selected, and the mice were randomly divided into four groups, each group containing 6 mice. They were injected intravenously with a dose of 5 mg/kg at the time points of 1, 5, and 9 days. The groups included: PBS (control group), RNP@SPF, Cu_2O@SPF, RNP@Cu_2O@SPF. After 21 days of treatment, the tumor tissue was removed, weighed and photographed, and preserved in 4% paraformaldehyde.

2.25. Genomic cleavage detection (GCD) assay

Genomic DNA from SW480 cells was isolated using DNAzol™ (Thermo Fisher Scientific Inc., 10503027) and amplified near the *ATP7A* target site using 2 × HyPerFUsion® High-Fidelity Master Mix (ApexBio Technology, K1039) and specific PCR primers. Primer sequences were indicated as below.

Primer sequences used for GCD:

ATP7A-F 5′-ACCCAAAAAACTTGAACTCTTTCTTAGG-3′

ATP7A-R 5′-GTGTCAGTAAAAAACAGATTTTGACTCC-3′

After denaturation and annealing of amplification products, the EnGen Mutation Detection Kit (NEB, E3321) was applied to identify indentation events. Subsequently, the frequency of these indentation events was quantified using ImageJ software (Image J2x 2.1.5.0, National Institutes of Health), and the gene editing efficiency of the target gene ATP7A *in vitro* and *in vivo* was evaluated using Eq. (1). The Sanger sequencing is entrusted to General Bio Corporation.

$$\text{Indel}\ (\%) = [\text{Sum of cleaved band intensities} / (\text{Sum of cleaved and parental band intensities})] \times 100 \quad (1)$$

2.26. Histology

The tumor specimens were wrapped in paraffin and cut into 2 μm sections for H&E staining and immunohistochemical analysis. Then, the sectioned DNA was detected with the terminal deoxynucleotidyl transferase-mediated dUTP nick-end labeling B(TUNEL) cell apoptosis detection kit fragments, observed for fluorescence, and quantitatively analyzed for cell apoptosis after administration of different nano-preparations.

2.27. Histopathology test

For *in vivo* biosafety assessment, equivalent doses of 0, 50, and 100 mg/kg of RNP@Cu_2O@SPF were injected into healthy BALB/c mice *via* the tail vein. The serum of the mice was collected within 24 h after intravenous injection, and blood routine analysis was performed, including measurements of ALB, ALT, TP, AST, ALP, and BUN. Three weeks after the RNP@Cu_2O@SPF injection, the major organs were removed, and both hematoxylin-eosin (H&E) staining and immunohistochemical staining were used for histopathological examination.

2.28. Statistical analysis

Statistical Product and Service Solutions (SPSS) 19.0 was used to evaluate the statistical data. An unpaired two-tailed Students' *t*-test was used to compare the difference between the two groups. One-way analysis of variance (ANOVA) was used to compare the differences among multiple groups. Two-way ANOVA with a Bonferroni *post hoc* test was used when both time and treatment were compared. Statistical significance was considered at $P < 0.05$. Data are presented as means ± standard deviation (SD). Differences of $^*P < 0.05$, $^{**}P < 0.01$, $^{***}P < 0.001$ were considered statistically significant.

The detailed experimental procedures are described in the Supporting Information.

3. Results and discussion

3.1. Synthetic and characterization of the RNP@Cu_2O@SPF

RNP@Cu_2O@SPF nanomedicine was synthesized as depicted in Scheme 1. Firstly, Cu_2O nanoparticle (NP) was synthesized according to the previous report[26]. Specifically, NaOH aqueous solution was injected into the $Cu(AC)_2$ and PEG mixed solution to form $Cu(OH)_2$ nanoparticles and then reduced to Cu_2O NPs with the addition of ascorbic acid (AA). As displayed in the scanning electron microscopy (SEM) image (Fig. 1A), the fabricated Cu_2O NPs exhibited a homogeneous sphere morphology with a mean size of about 82 nm. Next, the RNP was modified on Cu_2O nanoparticle due to the electrostatic interaction (RNP@Cu_2O). In the experiment, we used a relatively abundant amount of positively charged Cas9 protein, and even though the sgRNA carries a negative charge, the overall mixture was still positively charged. After RNP loading, the surface potential of the nanoparticle was transformed from negative (Cu_2O) to positive (RNP@Cu_2O), which was largely attributed to the covering of a positively charged complex. To protect RNP from degradation/leakage and achieve triggered release, RNP@Cu_2O was further encapsulated by organosilica shell (RNP@Cu_2O@S). Finally, the FA-coupled PEG was grafted on the RNP@Cu_2O@S surface through the condensation of hydroxyl and amino groups (RNP@Cu_2O@SPF)[27]. After the modification of the organosilica shell, the nanoparticle diameter increased to about 104 nm (Fig. 1B). The size distribution and corresponding PDI were measured through dynamic light scattering (DLS) and displayed in Fig. 1E and Supporting Information Fig. S1. The fabricated Cu_2O nanoparticles exhibited a uniform distribution and an average hydrated size of 86 nm. After the incubation with RNP and the modification of the organosilica shell, the hydrated particle size varied and increased to about 92 and 113 nm. The SEM elemental mapping results obviously displayed a core−shell structure and the existence of Cu, Si, O, and S elements in RNP@Cu_2O@SPF (Fig. 1D), which verified that organosilica was wrapped on Cu_2O triumphantly. Additionally, the zeta potential characterizations (Fig. 1C) of these nanoparticles exhibited obvious variations after each step of modification, which also confirmed the triumphant fabrication of these nanoparticles. The evaluation of loading efficiency, including loading content (RNP mass in nanoparticle/total mass of nanoparticle) and encapsulation efficiency (RNP mass in nanoparticle/added mass of RNP), was carried out by mixing different FITC labeled RNP concentration gradients (200, 400, and 800 μg/mL) with Cu_2O nanoparticles (1 mg/mL). After loading, the free RNP was measured by the fluorescence intensity of the supernatant, and, the total nanoparticle mass was measured by weighing post-concentrifugation. The encapsulation efficiency (loading content) was calculated to be 27.50% (8.40%), 35.00% (18.92%), and 21.87% (22.58%) within 6 h, respectively. Based on the abovementioned loading content and encapsulation efficiency, the optimal encapsulation efficiency was achieved at an RNP concentration of 400 μg/mL (Fig. 1F) while maintaining a relatively high loading content. Subsequently, the RNP release rate of RNP@Cu_2O@SPF was explored at different pH and GSH environments (pH = 7.4, pH = 7.4 + 10 mmol/L GSH, and pH = 5 + 10 mmol/L GSH), and the results revealed that the total cumulative release rate was 38% with 10 mmol/L GSH at pH = 7.4, which illustrated that GSH could trigger the degradation of organosilica shell through the breakage of disulfide bond. The RNP release rate further increased to about 78% in a weakly acidic environment (pH = 5), demonstrating the dissociation of Cu_2O nanostructure in weak acidic conditions (Fig. 1G). Afterward, the release capacity of Cu ion was evaluated by inductively coupled plasma-mass spectrometry (ICP-MS) under different pH environments with GSH. As exhibited in Fig. 1H, Cu ion was liberated fleetly under a weak acid environment (pH = 6.0 and 5.0), indicating that the release behavior of Cu ion had an acidic response. Furthermore, a more detailed study on the GSH consumption performance of RNP@Cu_2O@SPF was conducted by 5,5′-dithiobis (2-nitrobenzoic acid) (DTNB), which can be reduced to a yellow product with an absorption peak at 412 nm through GSH consumption. As displayed in Fig. 1I and Supporting Information Fig. S2, RNP@Cu_2O@SPF showed a time- and dose-dependent depletion of GSH, with the absorption peak at 412 nm of DTNB gradually decreased as the reaction time went on and the concentration of RNP@Cu_2O@SPF increased. Those outcomes are greatly encouraging because the excessive GSH and weak acidic features of TME could trigger the weak acidic and reductive responsive RNP and Cu^+ liberating and the succeeding inhibition of the expression of *ATP7A*, realizing the accumulation of intracellular Cu^+. The performance of the fabricated nanomedicine to initiate the Fenton-like reaction and convert H_2O_2 to harmful ·OH was also explored. Methylene blue (MB), which could be discolored and degraded by ·OH, was chosen as an indicator of ·OH generation in the Fenton-like reaction. As exhibited in Fig. 1J, single H_2O_2 seldom changed the absorption spectra of MB with GSH at pH = 5.0, while the RNP@Cu_2O@SPF nanoparticles-treated MB aqueous solution was degraded obviously, demonstrating the Cu^+ triggered Fenton-like reaction could usefully produce ·OH from H_2O_2 under the excessive GSH and weak acidic TME environment. These results revealed that RNP@Cu_2O@SPF nanoparticles could not only act as an efficient nanocarrier for RNP delivery but also act as a safe Cu^+ ions provider for cancer treatment.

3.2. The in vitro anti-tumor performance of RNP@Cu_2O@SPF

The methyl thiazolyl tetrazolium (MTT) assay was utilized to assess the viability of normal and cancer cells under the treatment of RNP@Cu_2O@SPF *in vitro*. The results in Fig. 2A and Supporting Information Fig. S3 demonstrated that the toxicity of nanomedicine to normal cells (SV-HUC-1 and FHC) was negligible, while showing significant damage to cancer cells (HT29 and SW480) with RNP@Cu_2O@SPF incubated at 50 μg/mL for 12 h. Then, the cell internalization efficiency of fluorescence-labeled (RITC-red fluorescence for silica, FITC-green fluorescence for RNP) RNP@Cu_2O@S and RNP@Cu_2O@SPF was investigated by confocal laser scanning microscopy (CLSM) and flow cytometry (FCM). According to CLSM images, cells in the RNP@Cu_2O@SPF group showed more pronounced green fluorescence (Cas9/FITC) and red fluorescence (silica/RITC) than those in the RNP@Cu_2O@S and the control groups. This could be explained by the targeting effect of FA that made RNP@Cu_2O@SPF more effectively endocytosed by SW480 cancer cells. Simultaneously, flow cytometry (FCM) results in Fig. 2B and C were consistent with the above CLSM images, with the fluorescence intensity of FITC in the RNP@Cu_2O@SPF group about 3-fold higher compared to the RNP@Cu_2O@S group (Supporting Information Fig. S4), indicating that FA modification can achieve targeted and efficient delivery of nanomedicine. Subsequently, the nanomedicine endocytic uptake pathway and mechanism were investigated by co-incubating RNP@Cu_2O@SPF with various endocytic pathway inhibitors, including chlorpromazine (CPZ), mycoplasma, dynasore,

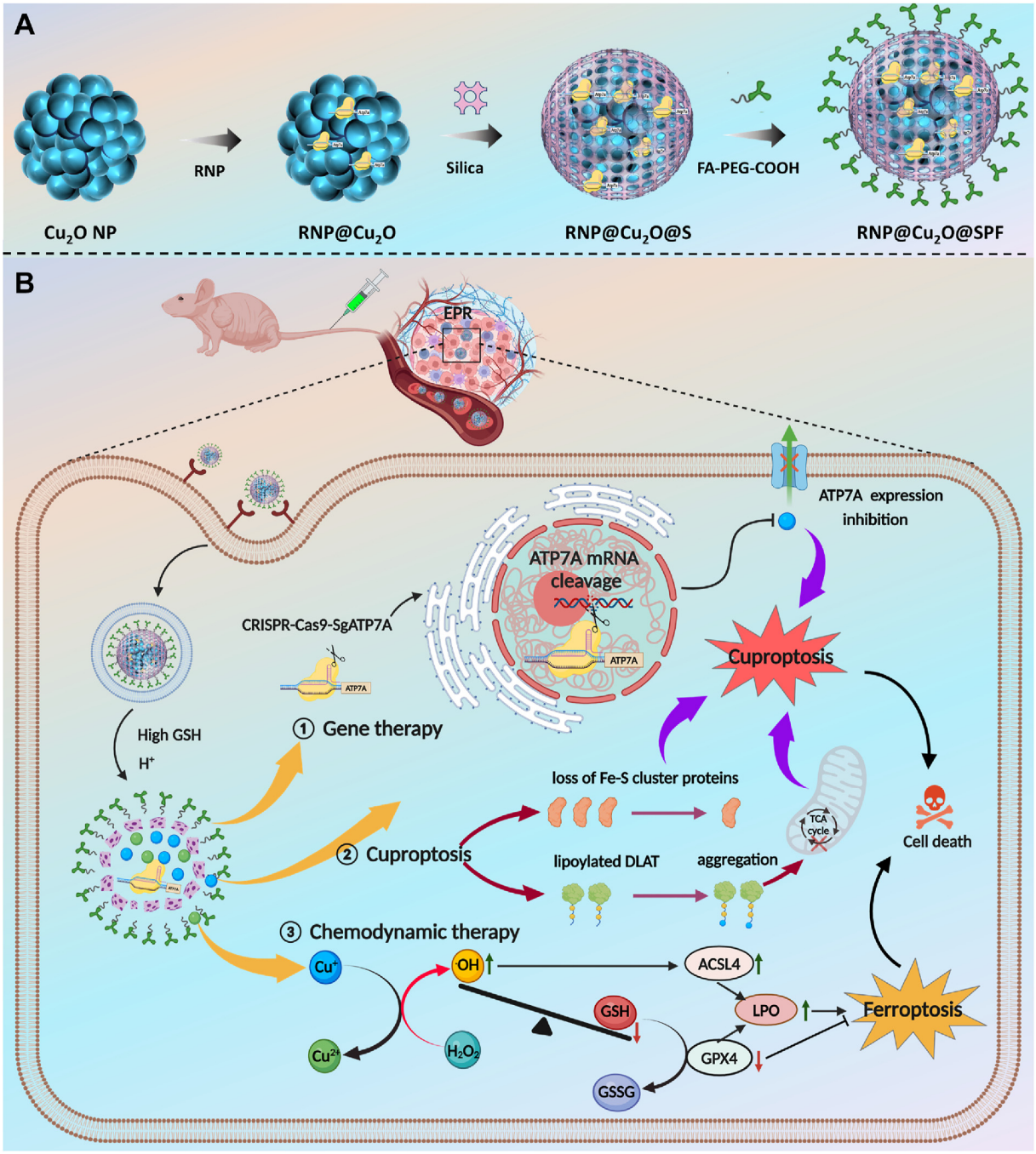

Scheme 1 (A) Schematics illustrating the step-by-step synthesis of the RNP@Cu_2O@SPF. (B) Diagram depicting the mechanism of gene editing enhanced cuproptosis/CDT/ferroptosis synergistic therapy.

amiloride, and β-cyclodextrin (CD). Immunofluorescence staining images and FCM analysis showed that the endocytosis efficiency of the nanomedicine was significantly reduced under the treatment of ATP synthesis inhibitors (NaN_3 and 4 °C) and clathrin-mediated endocytosis inhibitors, while other inhibitors rarely generated influence on cellular endocytosis (Supporting Information Fig. S5). The above result suggests that RNP@Cu_2O@SPF enters the cell mainly through adenosine 5′-triphosphate (ATP)-dependent or clathrin-mediated endocytosis.

ATP7A is a copper transporter P-type ATPase that can pump excess copper out of the cell when the intracellular copper level increases over its normal level, protecting the cell from copper toxicity[18]. In our experiment, RNP@Cu_2O@SPF was endocytosed by the cell and underwent lysosomal escape, accompanied by auto-degradation in response to acid and GSH to release RNP into the cytoplasm. Then, the cytoplasmic RNP was internalized by the nucleus to knock down the expression of the oncogene *ATP7A*, causing copper accumulation in the cytoplasm and boosting CDT, ferroptosis, and cuproptosis. In this regard, the editing efficiency of

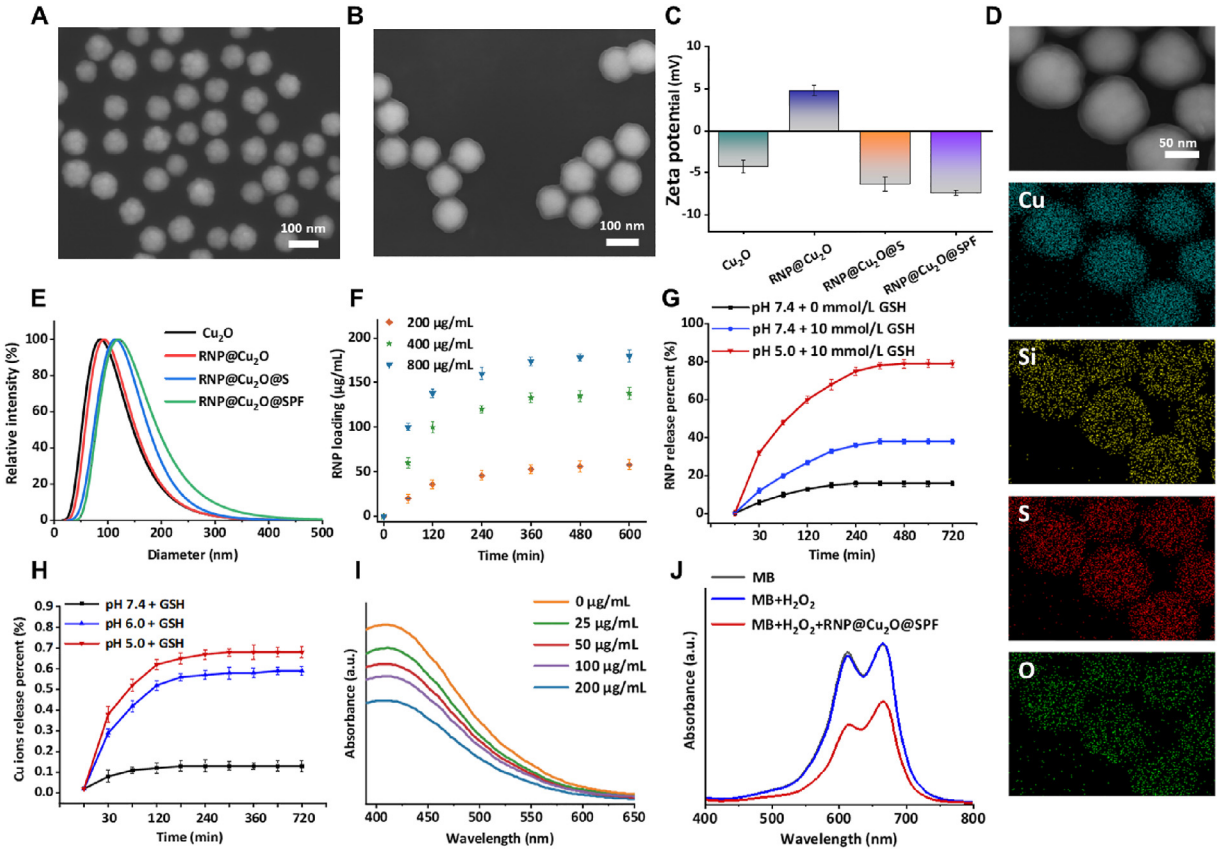

Figure 1 Characterization of RNP@Cu_2O@SPF. SEM image pictures of the Cu_2O (A) and RNP@Cu_2O@SPF (B) nanoparticles. Scale bar, 100 nm. (C) Zeta potential characterizations of Cu_2O, RNP@Cu_2O, RNP@Cu_2O@S, and RNP@Cu_2O@SPF. (D) The SEM element mapping images of RNP@Cu_2O@SPF nanoparticles. Scale bar, 50 nm. (E) DLS characterizations of Cu_2O, RNP@Cu_2O, RNP@Cu_2O@S and RNP@Cu_2O@SPF. (F) Incorporation abilities of RNP onto Cu_2O (1 mg/mL) at varying RNP dosages (200, 400, and 800 μg/mL). (G) Cumulative release of RNP from RNP@Cu_2O@SPF nanoparticles in the PBS medium at different GSH and pH environments. (H) Cu release abilities from the RNP@Cu_2O@SPF nanoparticles at various pH conditions with 10 mmol/L GSH. (I) UV−Vis absorption spectra of DTNB treated with different concentrations of RNP@Cu_2O@SPF nanoparticles in the presence of GSH. (J) UV−Vis absorption curves of MB treated with H_2O_2 and the RNP@Cu_2O@SPF nanoparticles under the GSH and weak acidic environment (pH 5 with 10 mmol/L GSH). The data are shown as mean ± SD (n = 6).

CRISPR-Cas9-Sg*ATP7A* delivered through RNP@Cu_2O@SPF was evaluated by genomic cleavage detection (GCD). As shown in Supporting Information Fig. S6, the frequency of indel events was 55.3% in the cells treated with RNP@Cu_2O@SPF. In addition, the Sanger sequencing experiments of the PCR amplicon of the targeted sites after various treatments were exhibited in Supporting Information Fig. S7. The control and Cu_2O@SPF groups revealed that the DNA fragment almost underlined was in the targeted locus, while the height of several main peaks varied and many miscellaneous peaks occurred with the treatment of RNP@Cu_2O@SPF, further validating the feasibility of RNP@Cu_2O@SPF regarding gene editing. Moreover, WB and immunofluorescence were also used to evaluate the release, internalization of the nucleus, and expression of RNP. In comparison to PBS control and Cu_2O@SPF groups, RNP@Cu_2O@SPF-treated SW480 cells showed an obvious down-expression of ATP7A (Fig. 2D and E). The Cu content in the cells was measured with a copper assay kit. It was found that the Cu content increased by about two-fold in the SW480 cells treated with RNP@Cu_2O@SPF when compared with Cu_2O@SPF-treated cells (Fig. 2F), which further verified the successful downregulation of ATP7A and accumulation of cooper in the cells. To evaluate the generation of ·OH after RNP@Cu_2O@SPF entered the cells, the 2′,7′-dichlorofluorescein diacetate (DCFH-DA), which can be oxidized to green fluorescent 2′,7′-dichlorofluorescein (DCF) by ·OH, was selected as a probe for the detection of ·OH. Specifically, SW480 cells were co-cultured with Cu_2O@SPF and different concentrations of RNP@Cu_2O@SPF, and the green fluorescence produced by DCF was detected by CLSM. The results exhibited that cells treated with Cu_2O@SPF showed faint green fluorescence compared with PBS-treated SW480 cells, while obviously enhanced after RNP@Cu_2O@SPF treatment, and it was further elevated with the enhancive incubation content of RNP@Cu_2O@SPF in Fig. 2G, demonstrating that the RNP could restrain the expression of *ATP7A* and realize the cumulation of Cu^+ to facilitate the disintegration of H_2O_2 to produce ROS. In addition, RNP@Cu_2O@SPF significantly depleted GSH, which was evidenced by the significant decrease in the GSH/GSSG ratio in Fig. 2H.

3.3. *The synergistic therapy mechanism of RNP@Cu_2O@SPF*

Encouraged by the splendid *in vitro* antitumor effect of RNP@Cu_2O@SPF, the multi-pathway synergistic mechanism was investigated. The schematic depicts the enhanced synergistic cuproptosis/CDT/ferroptosis therapy *via* gene editing (Fig. 3A).

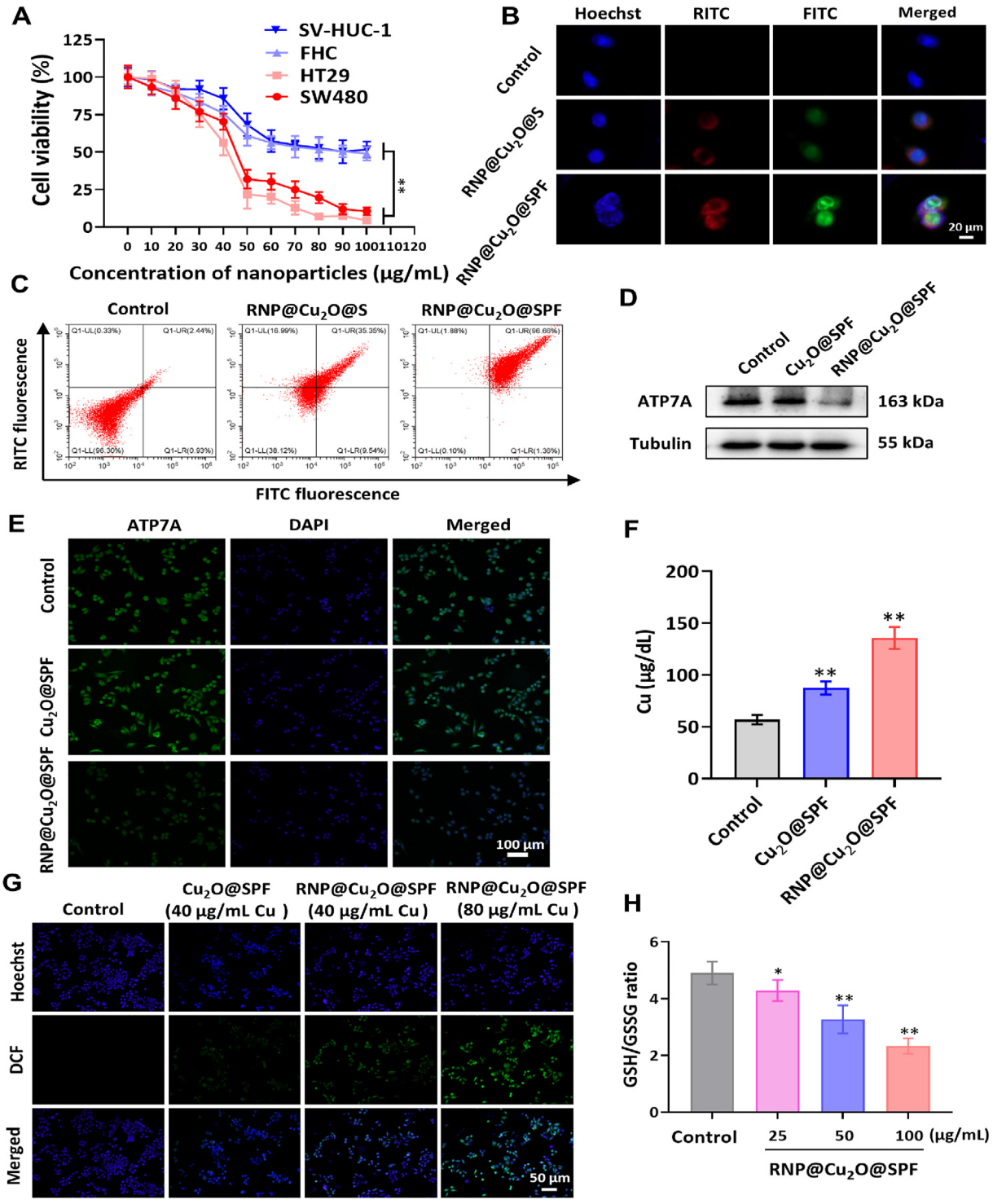

Figure 2 *In vitro* distribution and tumor-combatting effect of RNP@Cu_2O@SPF. (A) The viability of cancer and normal cells treated with RNP@Cu_2O@SPF for 24 h in the dark ($n = 6$). (B) CLSM images of SW480 cells incubated with RNP@Cu_2O@SPF or RNP@Cu_2O@S (FITC-labelled RNP, RITC-labelled silica). Scale bar, 20 μm. (C) FCM analysis showcasing transfection rates in SW480 cells after 4 h of immersion with PBS, RNP@Cu_2O@S, or RNP@Cu_2O@SPF. WB assay (D) and fluorescence imaging (E) of ATP7A expression in SW480 cells treated with RNP@Cu_2O@S or RNP@Cu_2O@SPF. Scale bar, 100 μm. (F) Relative copper contents in SW480 cells after a 24 h treatment with Cu_2O@SPF or RNP@Cu_2O@SPF ($n = 6$). (G) Fluorescence microscopy images of ROS generation in SW480 cells treated with PBS, Cu_2O@SPF(40 μg/mL), RNP@Cu_2O@SPF (40 μg/mL), and RNP@Cu_2O@SPF (80 μg/mL) for 4 h and stained with DCFH-DA to indicate the ROS generation. Scale bar, 50 μm. (H) GSH/GSSG ratio in SW480 cells treated with different concentrations of RNP@Cu_2O@SPF (25, 50, 100 μg/mL) for 6 h ($n = 6$). The data are shown as mean ± SD. ns, no significant; $^*P < 0.05$, $^{**}P < 0.01$.

The suggested mechanism was further validated by the subsequent experiments. Reportedly, the ·OH produced through the Fenton reaction could trigger the apoptosis in cancer cell[28−30]. Thus, Annexin V-FITC/PI double staining and flow cytometry (FCM) experiments were conducted. A more significant number of apoptotic cells (Annexin V^+/PI^-) were found in the RNP@Cu_2O@SPF group compared to Cu_2O@SPF and RNP@SPF groups (Fig. 3B and C), indicating that RNP@Cu_2O@SPF nanomedicine could efficiently initiate apoptosis pathways through accumulated Cu^+ and excess H_2O_2 triggered CDT.

Cuproptosis leads to the oligomerization of lipidated proteins in the mitochondrial tricarboxylic acid cycle and the loss of Fe−S cluster proteins through the copper cumulation in cells[4]. In MTT assays, RNP@Cu_2O@SPF-treated cells cultured with galactose exhibited more pronounced cytotoxic sensitivity than those cultured in glucose medium (Fig. 3D). Subsequently, mitochondrial uncoupler FCCP, antimycin A (an electron transport chain inhibitor) and electron transport inhibitor rotenone were added, respectively. As displayed in Fig. 3E, FCCP seldom had effects on cell viability, while antimycin A and rotenone significantly rescued the cell killing induced by RNP@Cu_2O@SPF. Those results suggested that RNP@Cu2O@SPF-induced cell death relies on mitochondrial respiration rather than ATP. Besides, the addition of UK5099 or antimycin A exhibited a similar rescue effect on cancer cells (Fig. 3F). Next, the cell colony and invasion experiments exhibited that SW480 cells in the RNP@Cu_2O@SPF group showed superior inhibition of cell proliferation and invasion than those in the Cu_2O@SPF and RNP@SPF groups, while the suppression effect obviously decreased after the addition of cuproptosis inhibitor-UK5099. The above experimental results indicated that RNP@Cu_2O@SPF could activate the cuproptosis pathway to inhibit the growth of SW480 cancer cells (Supporting Information Figs. S8 and S9). Besides, the copper chelator tetrathiomolybdate (TTM) treatment experiment results showed that cancer cells were rescued by the addition of TTM, and the number of cells rescued was proportional to the dose of TTM, which further confirmed that the anticancer effect of RNP@Cu_2O@SPF was closely related to intracellular copper content (Fig. 3G). The subsequent obtained WB result was consistent with protein expression in the classical pathway of cuproptosis, where copper binding to dihydrolipoamide *S*-acetyltransferase (DLAT) caused oligomerization (Fig. 3H). In addition, the Fe−S cluster proteins ferredoxin (FDX1), lipoic acid synthase (LIAS), aconitic acid hydratase 2 (ACO-2), succinate dehydrogenase subunit B (SDHB) and lipoic acid DLST (lip-DLST) were also downregulated in SW480 cells after treatment with nanomedicine (Fig. 3I). These results illustrated that the RNP@Cu_2O@SPF nanomedicine could trigger the cuproptosis pathway for killing cancer cell.

Recent literature has proposed that excessive intracellular copper can induce ferroptosis, a kind of programmed cell death that is characterized by GSH depletion and lipid peroxidation (LPO) accumulation. Ferroptosis could be regulated by glutathione peroxidase 4 (GPX4) and acyl-CoA synthetase long-chain family member 4 (ACSL4)[31−33]. Cellular immunofluorescence and WB images illustrated that the gene expression of GPX4 in CRC SW480 cells gradually decreased with the increased nanomedicine dosage (Fig. 3J−M and Supporting Information Fig. S10), while the expression of LPO displayed the opposite trend. WB results further demonstrated that the expression of GPX4 decreased and the expression of ACSL4 increased when the nanomedicine dosage enhanced (Fig. 3K and Supporting Information Fig. S11). Besides, after the addition of ferroptosis inhibitor DFO, a noticeable reversal of cell viability was observed (Fig. 3L). Cell migration, colony, and invasion experiments in Supporting Information Fig. S12 displayed that SW480 cells in the RNP@Cu_2O@SPF group revealed greater inhibition of cell migration, proliferation, and invasion than those in the control group, while the inhibition effect distinctly decreased after the addition of ferroptosis inhibitor-DFO. These results evidently demonstrated that the ferroptosis triggered by RNP@Cu_2O@SPF contributes to excellent anticancer performance. In summary, the gene editing enhanced nanotherapeutic strategy exhibited great prospects for cuproptosis/CDT/ferroptosis synergetic CRC therapy.

3.4. *The in vivo study of RNP@Cu_2O@SPF for tumor synergistic combination therapy*

Inspired by the significant efficiency of killing cancer cells by RNP@Cu_2O@SPF *in vitro*, *in vivo* experiments using BALB/c tumor-bearing mice were conducted to verify the synergistic therapeutic effects of RNP@Cu_2O@SPF (Fig. 4A). First, to study the tumor-targeted delivery behavior of RNP@Cu_2O@SPF, mice were intravenously injected with RNP@Cu_2O@S and RNP@Cu_2O@SPF for *in vivo* fluorescence imaging at different time points (1, 4, 12, 24 and 48 h). *Ex vivo* fluorescence imaging of tumors and major organs was collected 24 h after injection. After 48 h, the biodistribution of non-targeted and targeted groups on major organs and tumors of mice was analyzed semi-quantitatively by *in vitro* imaging. The results showed that the fluorescence intensity of the RNP@Cu_2O@SPF group in tumor tissue was always higher than that of the RNP@Cu_2O@S group (Fig. 4B), which was consistent with the FCM quantitative results (Fig. 4C and Supporting Information Fig. S13). These results illustrated that RNP@Cu_2O@SPF could deliver and cumulate effectually and directionally in tumor sites, enhancing permeability, retention (EPR) effects, and overexpressed FA receptors on SW480 cells. Additionally, the Cu and Si accumulation results in Supporting Information Fig. S14 demonstrated that RNP@Cu_2O@SPF was mainly distributed in the tumor, liver, lung, and kidney, and the highest tumor accumulation was achieved at about 24 h after injection, which supplied the suitable treatment time for cancer therapy. Further, the therapeutic effect of RNP@Cu_2O@SPF *in vivo* was conducted. BALB/c tumor-bearing mice were divided into four groups treated with PBS, RNP@SPF, Cu_2O@SPF, and RNP@Cu_2O@SPF, respectively ($n = 6$). The mice were euthanized after 21 days of treatment, and tumor tissue samples were collected and measured. The tumor volumes increased rapidly in the control, Cu_2O@SPF, and RNP@SPF groups, illustrating the limited therapeutic effect of these nanomedicines. However, RNP@Cu_2O@SPF obviously inhibited tumor growth and improved mice survival rate (Fig. 4D−F and Fig. 4J), which was attributed to the synergistic multiple therapeutic effects. Additionally, H&E staining of tumor tissues revealed more cell death in the RNP@Cu_2O@SPF group (Fig. 4I). In general, the synergistic therapy based on RNP@Cu_2O@SPF nanomedicine, which combines gene editing with cuproptosis/CDT/ferroptosis, demonstrates the potential for significant tumor suppression. Subsequently, the GCD assay, Sanger sequencing analysis, WB, and immunohistochemistry experiments were carried out to illustrate the tumor repressive effect of gene editing suppressed *ATP7A* expression for enhanced cuproptosis/CDT/ferroptosis. The GCD in Supporting Information Fig. S15 showed that the gene editing frequency of indel events was 25.5% in tumor tissue, and *in vivo* Sanger

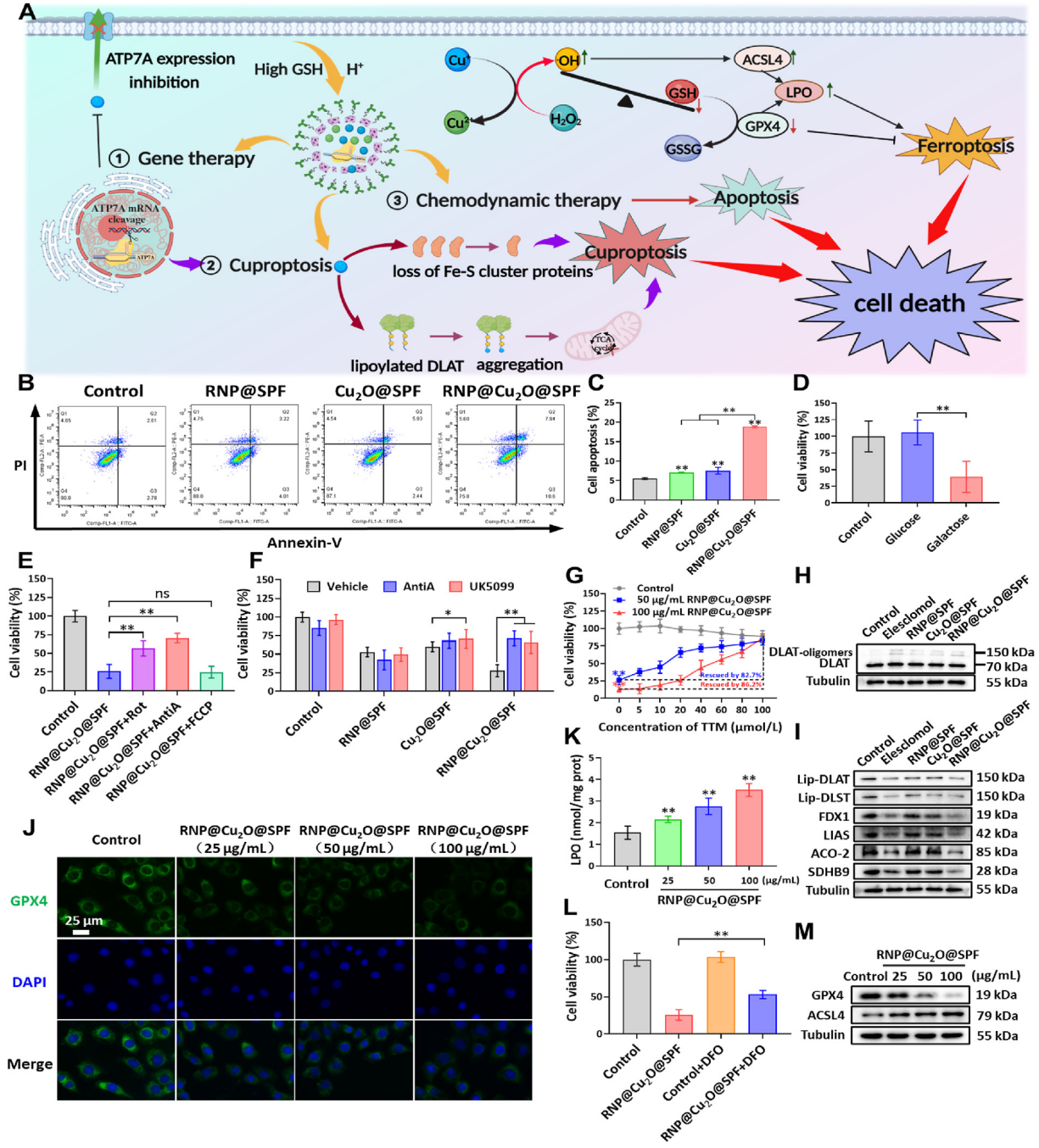

Figure 3 Anti-tumor mechanisms studies of RNP@Cu_2O@SPF. (A) The schematic diagram of cell death mechanisms of RNP@Cu_2O@SPF nanomedicine-mediated synergetic therapy. (B) FCM analysis with Annexin V-FITC/PI dual labels on SW480 cells after 24 h of incubation with different nanoparticles. (C) The percentages of cells undergoing apoptosis (%) in different groups ($n = 3$). (D) Viability of SW480 cells grown in media containing either glucose or galactose treated with RNP@Cu_2O@SPF (ratio 1:1) ($n = 6$). (E) Viability of SW480 cells pretreated with 0.1 mmol/L rotenone (Rot), 0.1 mmol/L antimycin A (anti-A), or 1 mmol/L FCCP and then treated with RNP@Cu_2O@SPF ($n = 6$). (F) Viability of SW480 cells post-treated with Antimycin A or UK5099 under different conditions (incubated with various nanoparticles) ($n = 6$). (G) Viability of SW480 cells treated with tetrathiomolybdate in different concentrations of RNP@Cu_2O@SPF (50, 100 μg/mL) ($n = 6$). (H) Western blot analysis of DLAT-oligomers, DLAT, and Tubulin expression levels in SW480 cells after treatment with different nanoparticles. (I) Western blot analysis of lipoylated proteins, FDX1, LIAS, ACO-2, SDHB9, and Tubulin expression levels in SW480 cells after treatment with different nanoparticles. (J) Fluorescence depiction of GPX4 levels in SW480 cells post RNP@Cu_2O@SPF treatment at different dosages (25, 50, and 100 μg/mL) for 24 h. Scale bar, 25 μm. (K) LPO contents in SW480 cells treated with RNP@Cu_2O@SPF at different concentrations (25, 50, and 100 μg/mL) for 24 h ($n = 6$). (L) Survival rates of SW480 cells after 24 h of incubation with solutions of PBS, RNP@Cu_2O@SPF, PBS+DFO, or RNP@Cu_2O@SPF+DFO ($n = 6$). (M) WB assay of GPX4, ACSL4, and Tubulin expression in SW480 cells treated with RNP@Cu_2O@SPF at varied concentrations (25, 50, and 100 μg/mL) for 24 h. The data are shown as mean ± SD. ns, not significant; $^*P < 0.05$, $^{**}P < 0.01$.

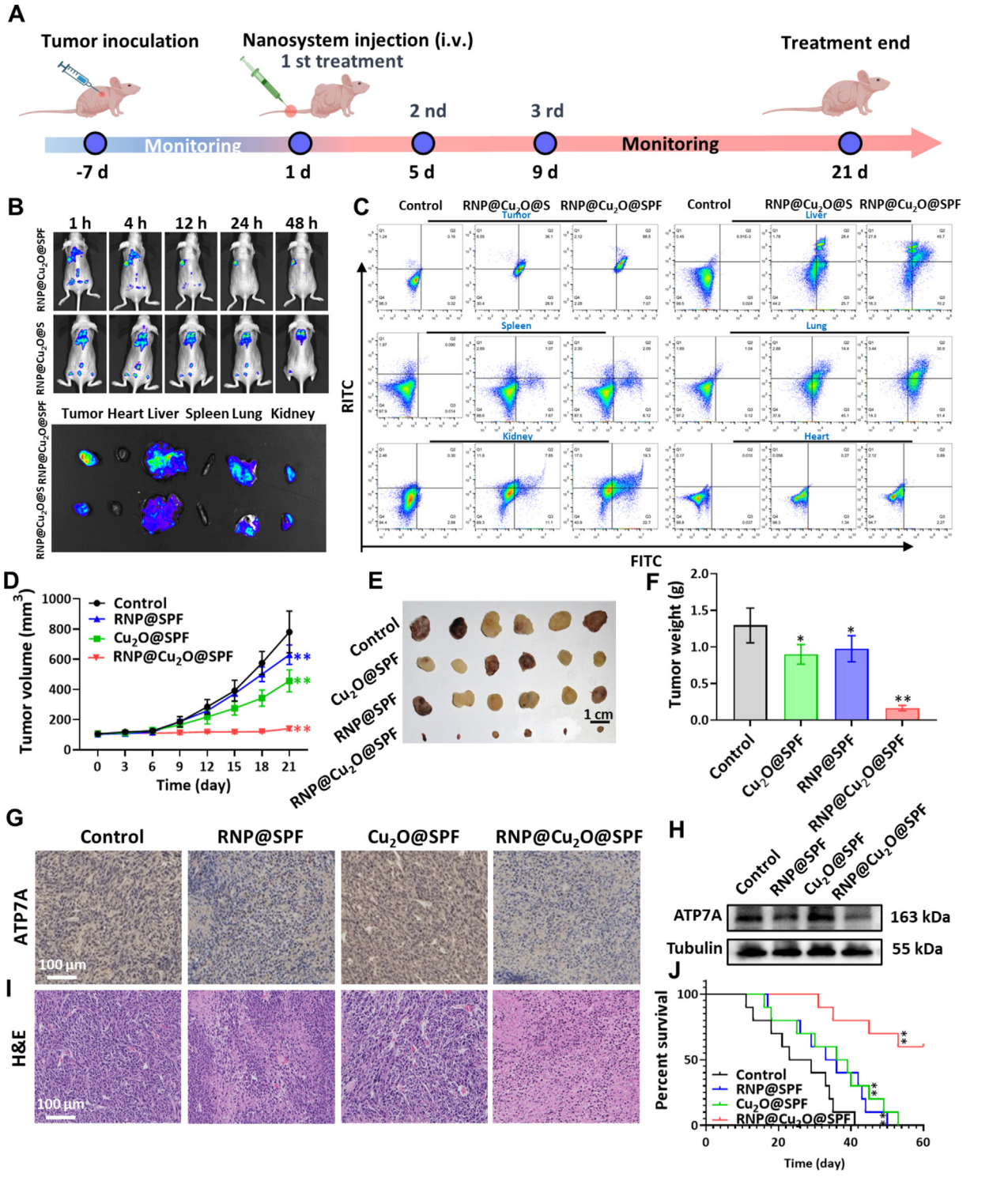

Figure 4 *In vivo* examination of RNP@Cu_2O@SPF for collaborative tumor therapy. (A) Pictorial representation of the *in vivo* therapeutic approach. (B) Live fluorescence visuals of mice post-injected with standalone RITC and RNP@Cu_2O@SPF across various intervals and external fluorescence visuals of the tumor and primary organs 24 h after injection. (C) The absorption efficiency of RNP@Cu_2O@S or RNP@Cu_2O@SPF into primary organs and tumors and the associated average fluorescence intensity determined by FCM after 24 h. (D) Tumor progression trends throughout the therapeutic period ($n = 6$). (E) Images of tumors extracted from mice upon concluding the therapy. Scale bar, 1 cm. (F) Ultimate weight of the excised tumors upon concluding the therapy ($n = 6$). (G) ATP7A labeling of tumor slices. (H) WB was employed to ascertain ATP7A concentration in tumor specimens. Scale bar, 100 μm. (I) H&E labeled tumor samples post varied therapies. Scale bar, 100 μm. (J) Survival rates of the mice in different treatment groups ($n = 10$). The data are shown as mean ± SD. ns, not significant; $^*P < 0.05$, $^{**}P < 0.01$.

sequencing experiments exhibited that the height of several main peaks varied and many miscellaneous peaks obviously occurred with the treatment of RNP@Cu_2O@SPF (Supporting Information Fig. S16). Besides, a distinct downregulated ATP7A protein (Fig. 4H and Supporting Information Fig. S17) was also observed in the RNP@Cu_2O@SPF group, verifying the triumphant gene editing *via the* CRISPR Cas-9 system. Meanwhile, immunohistochemical staining of ATP7A at tumor tissues exhibited analogical results (Fig. 4G). Besides, high ROS expression and a low ratio of GSH/GSSG in tumor tissue indicated the strong GSH depletion capability and good ·OH generation ability of RNP@CuP@SPF, which can disrupt the antioxidant state within tumor cells (Supporting Information Figs. S18 and S19). TUNEL staining was employed to detect apoptosis in tumor cells. The results showed that the RNP@Cu_2O@SPF group with gene editing enhanced synergistic therapy exhibited the highest apoptosis rate (Supporting Information Fig. S20). The above results confirmed the splendid capacity of RNP@Cu_2O@SPF nanomedicine for gene editing enhanced synergistic cuproptosis/CDT/ferroptosis therapy.

The prepared nanomedicine should not only have a good therapeutic effect, but also have good biosafety. Healthy BALB/c mice were injected with RNP@Cu_2O@SPF and seldom significant weight variation was found in all groups after half a month, suggesting that RNP@Cu_2O@SPF had no potential systemic toxicity (Supporting Information Fig. S21). In Fig. 4J, the therapy duration was extended to 60 days to exclude the potential effect of the duration of administration on the toxicity of mice. The impact of RNP@Cu_2O@SPF on liver and kidney function markers was evaluated through blood biochemical and whole-blood sample analyses. Compared to the control group, the levels of albumin (ALB), alanine aminotransferase (ALT), total protein (TP), aspartate aminotransferase (AST), alkaline phosphatase (ALP), and blood urea nitrogen (BUN) in the RNP@Cu_2O@SPF treatment groups showed no abnormal changes on average (Supporting Information Fig. S22). Besides, the highly specific CRISPR/Cas9 system with ignorable off-target risk was important. To further verify the biosafety of the constructed nanomedicine, the ATP7A protein expression in major organs was evaluated through ATP7A staining experiments. In Supporting Information Fig. S23B, the ATP7A expression of major organs (heart, liver, spleen, lung, and kidney) collected from the tumor-beard mice treated with RNP@Cu_2O@SPF at different concentrations (0, 5, and 50 mg/kg) showed no significant variations, indicating the nanomedicine could not liberate the RNP for efficient gene editing in major organs, while only release within the tumor sites with excess GSH and weak acidic environment for gene editing. Furthermore, no obvious damage on major organs (heart, liver, spleen, lung, and kidney) was found in H&E staining (Fig. S23A), which illustrated the pleasant biosafety of the prepared nanoplatforms.

4. Conclusions

In this study, we have creatively designed and synthesized RNP@Cu_2O@SPF nanoparticle as the nanotherapeutic vector of CRISPR-Cas9 to achieve gene editing enhanced cuproptosis/CDT/ferroptosis synergistic therapy. The nanomedicine was internalized into cancer cells through the EPR and FA targeted effect and displayed GSH and weak acid dual-responsive degradation behavior. Cu^+ liberated from Cu_2O efficaciously initiated the Fenton-like reaction and triggered the cuproptosis by causing DLAT aggregation. The ·OH generated *via* CDT promoted the GSH depletion, which facilitated the LPO accumulation and GPX4 deactivation for the ferroptosis metabolic pathway. Moreover, the released RNP could elevate the Copper-based therapy pathways by restraining the *ATP7A* expression, which allowed the accumulation of copper in the cytoplasm for stimulated synergistic cuproptosis/CDT/ferroptosis. The experimental results exhibited the admirable tumor inhibition ability of RNP@Cu_2O@SPF with favorable biosafety. In short, the established therapy nanoplatforms supply a reformatory and convenient strategy for CRISPR-Cas9 mediated gene editing enhanced synergistic cuproptosis/CDT/ferroptosis therapy, which provides a new way of thinking and direction for tumor treatment based on cooper nanomaterials.

Acknowledgments

The work was supported by the National Natural Science Foundation of China (82374287, 82174466, 81930117), National Key Research and Development Project (2022YFC3500200, China), Key research and development projects of Ningxia (Grant No. 2021BEG02040, China), Natural Science Foundation Project of Jiangsu Province (BK20211390, China), Open Projects of the Discipline of Chinese Medicine of Nanjing University of Chinese Medicine Supported by the Subject of Academic priority discipline of Jiangsu Higher Education Institutions, Program for Leading Talents of Traditional Chinese Medicine of Jiangsu Province (SLJ0314), and Blue Project of Jiangsu province.

Author contributions

Xiaoyu Wu, Zijun Bai, and Hui Wang designed and conducted the whole experiment, Hanqing Wang and Dahai Hou conducted the characterization experiments, Yunzhu Xu and Guanqun Wo analyzed the experiment results, Haibo Cheng, Dongdong Sun and Weiwei Tao drafted and revised the final manuscript. All authors read and approved the final manuscript.

Conflicts of interest

The authors declare no competing financial interest.

Appendix A. Supporting information

Supporting information to this article can be found online at https://doi.org/10.1016/j.apsb.2024.05.029.

References

1. Morgan E, Arnold M, Gini A, Lorenzoni V, Cabasag CJ, Laversanne M, et al. Global burden of colorectal cancer in 2020 and 2040: incidence and mortality estimates from GLOBOCAN. *Gut* 2023;**72**:338–44.
2. Siegel RL, Miller KD, Jemal A. Cancer statistics, 2020. *CA Cancer J Clin* 2020;**70**:7–30.
3. Rejhová A, Opattová A, Čumová A, Slíva D, Vodička P. Natural compounds and combination therapy in colorectal cancer treatment. *Eur J Med Chem* 2018;**144**:582–94.
4. Zhang XY, Li JF, Wang X, Wang YY, Hang RQ, Huang XB, et al. Effects of copper nanoparticles in porous TiO_2 coatings on bacterial resistance and cytocompatibility of osteoblasts and endothelial cells. *Mater Sci Eng C* 2018;**82**:110–20.
5. Tsvetkov P, Coy S, Petrova B, Dreishpoon M, Verma A, Abdusamad M, et al. Copper induces cell death by targeting lipoylated TCA cycle proteins. *Science* 2022;**375**:1254–61.

6. Li SR, Bu LL, Cai LL. Cuproptosis: lipoylated TCA cycle proteins-mediated novel cell death pathway. *Signal Transduct Target Ther* 2022;**7**:158.
7. Ning SP, Lyu M, Zhu DM, Lam JWY, Huang QQ, Zhang TF, et al. Type-I AIE photosensitizer loaded biomimetic system boosting cuproptosis to inhibit breast cancer metastasis and rechallenge. *ACS Nano* 2023;**17**:10206−17.
8. Tang ZM, Zhao PR, Wang H, Liu YY, Bu WB. Biomedicine meets fenton chemistry. *Chem Rev* 2021;**121**:1981−2019.
9. Jia CZ, Wu H, Luo KY, Hao WJ, Wang SG, Huang MX. Magnetic silica nanosystems with NIR-responsive and redox reaction capacity for drug delivery and tumor therapy. *Front Chem* 2020;**8**:567652.
10. Zhang GL, Xie WT, Xu ZW, Si YC, Li QD, Qi XY, et al. CuO dot-decorated Cu@Gd_2O_3 core−shell hierarchical structure for Cu(I) self-supplying chemodynamic therapy in combination with MRI-guided photothermal synergistic therapy. *Mater Horizons* 2021;**8**:1017−28.
11. Zhang CY, Yan L, Wang X, Dong XH, Zhou RY, Gu ZJ, et al. Tumor microenvironment-responsive $Cu_2(OH)PO_4$ nanocrystals for selective and controllable radiosentization *via* the X-ray-triggered fenton-like reaction. *Nano Lett* 2019;**19**:1749−57.
12. Sun XF, Ou ZH, Chen RC, Niu XH, Chen D, Kang R, et al. Activation of the p62-Keap1-NRF2 pathway protects against ferroptosis in hepatocellular carcinoma cells. *Hepatology* 2015;**63**:173−84.
13. Liu YW, Huang P, Li Z, Xu CH, Wang HZ, Jia BQ, et al. Vitamin C sensitizes pancreatic cancer cells to erastin-induced ferroptosis by activating the AMPK/Nrf2/HMOX1 pathway. *Oxid Med Cel Longev* 2022;**2022**:1−15.
14. Ta N, Qu CR, Wu H, Zhang D, Sun TT, Li YJ, et al. Mitochondrial outer membrane protein FUNDC2 promotes ferroptosis and contributes to doxorubicin-induced cardiomyopathy. *Proc Natl Acad Sci U S A* 2022;**119**:e2117396119.
15. Friedmann Angeli JP, Schneider M, Proneth B, Tyurina YY, Tyurin VA, Hammond VJ, et al. Inactivation of the ferroptosis regulator Gpx4 triggers acute renal failure in mice. *Nat Cel Biol* 2014;**16**:1180−91.
16. Doll S, Proneth B, Tyurina YY, Panzilius E, Kobayashi S, Ingold I, et al. ACSL4 dictates ferroptosis sensitivity by shaping cellular lipid composition. *Nat Chem Biol* 2016;**13**:91−8.
17. Xie JM, Yang YN, Gao YB, He J. Cuproptosis: mechanisms and links with cancers. *Mol Cancer* 2023;**22**:46.
18. Kaler SG. ATP7A-related copper transport diseases—emerging concepts and future trends. *Nat Rev Neuro* 2011;**7**:15−29.
19. Gu WX, Meng FH, Haag R, Zhong ZY. Actively targeted nanomedicines for precision cancer therapy: concept, construction, challenges and clinical translation. *J Control Release* 2021;**329**:676−95.
20. Fajrial AK, He QQ, Wirusanti NI, Slansky JE, Ding X. A review of emerging physical transfection methods for CRISPR/Cas9-mediated gene editing. *Theranostics* 2020;**10**:5532−49.
21. Ban Q, Yang P, Chou SJ, Qiao L, Xia HD, Xue JJ, et al. Supramolecular nanosubstrate-mediated delivery for CRISPR/Cas9 gene disruption and deletion. *Small* 2021;**17**:e2100546.
22. Li L, Hu S, Chen XY. Non-viral delivery systems for CRISPR/Cas9-based genome editing: challenges and opportunities. *Biomaterials* 2018;**171**:207−18.
23. Tao WW, Cheng XL, Sun DD, Guo Y, Wang N, Ruan J, et al. Synthesis of multi-branched Au nanocomposites with distinct plasmon resonance in NIR-II window and controlled CRISPR-Cas9 delivery for synergistic gene-photothermal therapy. *Biomaterials* 2022;**287**:121621.
24. Li XQ, Pan YC, Chen C, Gao YF, Liu XL, Yang KY, et al. Hypoxia-responsive gene editing to reduce tumor thermal tolerance for mild-photothermal therapy. *Angew Chem Int Ed* 2021;**60**:21200−4.
25. Chen C, Ma YP, Du SY, Wu YY, Shen PL, Yan T, et al. Controlled CRISPR-Cas9 ribonucleoprotein delivery for sensitized photothermal therapy. *Small* 2021;**17**:2101155.
26. Wu HS, Chen FH, You CQ, Zhang Y, Sun BW, Zhu Q. Smart porous core-shell cuprous oxide nanocatalyst with high biocompatibility for acid-triggered chemo/chemodynamic synergistic therapy. *Small* 2020;**16**:e2001805.
27. Prasetyanto EA, Bertucci A, Septiadi D, Corradini R, Castro-Hartmann P, De Cola L. Breakable hybrid organosilica nanocapsules for protein delivery. *Angew Chem Int Ed* 2016;**55**:3323−7.
28. Liu YT, Zhang J, Du J, Song K, Liu JL, Wang X, et al. Biodegradable BiOCl platform for oxidative stress injury−enhanced chemodynamic/radiation therapy of hypoxic tumors. *Acta Biomater* 2021;**129**:280−92.
29. Liu T, Xiong CF, Zhang LJ, Jiao GH, Shi H, Feng J, et al. Boosting doxorubicin-induced mitochondria apoptosis for the monodrug-mediated combination of chemotherapy and chemodynamic therapy. *Adv Healthc Mater* 2023;**12**:2202045.
30. Yu H, Zhao HY, Zhang YJ, Hou YM, Li RQ, Liang T, et al. A biomimetic nanoreactor for combinational chemo/chemodynamic therapy of choriocarcinoma through synergistic apoptosis and ferroptosis strategy. *Chem Eng J* 2023;**472**:144690.
31. Song WF, Zeng JY, Ji P, Han ZY, Sun YX, Zhang XZ. Self-assembled copper-based nanoparticles for glutathione activated and enzymatic cascade-enhanced ferroptosis and immunotherapy in cancer treatment. *Small* 2023;**19**:2301148.
32. Huang L, Zhu JY, Xiong W, Feng J, Yang J, Lu XY, et al. Tumor-generated reactive oxygen species storm for high-performance ferroptosis therapy. *ACS Nano* 2023;**17**:11492−506.
33. Li K, Lin CC, Li MH, Xu K, He Y, Mao YL, et al. Multienzyme-like reactivity cooperatively impairs glutathione peroxidase 4 and ferroptosis suppressor protein 1 pathways in triple-negative breast cancer for sensitized ferroptosis therapy. *ACS Nano* 2022;**16**:2381−98.